IEEE Access
Multidisciplinary | Rapid Review | Open Access Journal

Received April 7, 2019, accepted May 23, 2019, date of publication May 27, 2019, date of current version June 11, 2019.

Digital Object Identifier 10.1109/ACCESS.2019.2919224

Performance Analysis of Acoustic Emission Hit Detection Methods Using Time Features

FERNANDO PIÑAL MOCTEZUMA, (Student Member, IEEE), MIGUEL DELGADO PRIETO, (Member, IEEE), AND LUIS ROMERAL MARTÍNEZ, (Member, IEEE)

MCIA Research Center, Department of Electronic Engineering, Universitat Politècnica de Catalunya, 08222 Terrassa, Spain

Corresponding author: Fernando Piñal Moctezuma (juan.fernando.pinal@upc.edu)

This work was supported in part by the CONACYT Scholarship under Grant 411711, Mexico, and in part by the Ministry of Economy and Competitiveness Research Project, Spain, under Grant TRA2016-80472-R.

ABSTRACT Acoustic emission (AE) analysis is a powerful potential characterization method for fracture mechanism analysis during metallic specimen testing. Nevertheless, identifying and extracting each event when analyzing the raw signal remains a major challenge. Typically, the AE detection is carried out using a thresholding approach. However, though extensively applied, this approach presents some critical limitations due to overlapping transients, differences in strength and low signal-to-noise ratio. In this paper, to address these limitations, advanced methodologies for detecting AE hits have been developed. The most prominent methodologies used are instantaneous amplitude, the short-term average to long-term average ratio, the Akaike information criterion, and wavelet analysis, each of which exhibits satisfactory performance and ease of implementation for diverse applications. However, their proneness to errors in the presence of non-cyclostationary AE wavefronts and the lack of thorough comparison for transient AE signals are constraints to the wider application of these methods in non-destructive testing procedures. In this paper, with the aim of making aware of the drawbacks of the traditional threshold approach, a comprehensive analysis of its limiting factors when taking into regard the AE waveform behavior is presented. In addition, in a second section, a performance analysis of the main advanced representative-methods in the field is carried out through a common comparative framework, by analyzing first, AE waves generated from a standardized Hsu-Nielsen test and second, a data frame of a highly active signal derived from a tensile test. In this paper, with the aim to quantify the performance with which these AE detection methodologies work, for the first time, time features as the endpoint and duration accuracies, as well as statistical metrics as accuracy, precision, and false detection rates, are studied.

INDEX TERMS Acoustic emission, materials testing, AE thresholding method, short-term average to long-term average ratio, instantaneous amplitude, Akaike information criterion, wavelet analysis, Otsu's method.

I. INTRODUCTION

High demands are placed on safety and reliability specifications in the design and manufacturing of metallic materials, particularly in the transportation sector, where the lifetime, performance and cost of structural parts are critical aspects. This has led to extensive scientific and technical study of the mechanical properties of metallic components [1], [2].

Characterisation of the mechanical properties of metallic components commonly requires estimations of the post-yield strength, the tensile strength and the elongation of metallic specimens, which are evaluated through a standardized tensile test [3], [4]. This takes the form of a relatively simple destructive assay, which typically consists in fastening (either gripped or screwed) the specimen at the clamps of the apparatus and pulling until it breaks. Outcomes for the assay usually include records of the applied load force and the strain experienced by the specimen.

Determination of the plastic strain evolution exhibited by the specimen is critical to estimating the actual properties of the metallic material. Video extensometer-based systems are used to record the test, enabling visual forensic analysis to

The associate editor coordinating the review of this manuscript and approving it for publication was Dusmanta Kumar Mohanta.

be conducted. However, this approach has two main drawbacks: the frame digitization period, which is usually in the order of milliseconds, and the restriction to surface monitoring, which implies a significant loss of information about internal dislocations [5].

In recent years, the analysis of the acoustic emission (AE) phenomenon has been included as an additional mechanical descriptor to enhance the characterization capabilities of the assay [6]. Acoustic emission methods detect, locate or assess damage by means of the sudden materialization of elastic waves on the inspected material. These waves are the final effect of a previous process by which the mechanical capabilities of the material are surpassed with the application of a stress field. Therefore, the manifestation of each AE wave reflects an irreversible change in the crystalline structure of the material. This is an active field of research [7]; however, in order to conduct such an analysis, proper detection and capture of every AE event is highly desirable.

In order to automatically detect the AE events, also known as hits the most frequently used technique is to compare the obtained electrical signal against a predefined voltage threshold level; whenever the signal rises above this threshold, a hit has been detected. This technique was used in the first applications of AE as an evaluation tool and emerged due to the lack of digital hardware capable of handling the payload from the large data stream required for proper digital processing of the near-baseband signal [8].

With the advent of fully digital platforms, and given the relative efficiency and ease of implementation, nearly all the established standards for AE [9], [10], as well as commercially available instrumentation (and, as a result, most field work), use the threshold voltage technique as the default for AE activity detection. However, although it has not been exhaustively analyzed in the literature, the threshold method has critical drawbacks and limitations that could impair performance in the case of an irregular AE waveform.

Typically, once a set of AE hits has been detected, different features of each hit are extracted in order to locate or assess damage to the specimen. As might be expected, the more accurate and precise the detection, the better the quality of the subsequent evaluation [11]. Indeed, in recent years, significant efforts have been made to develop advanced signal processing approaches for better AE hit detection outcomes [12], [13].

Due to similarities in the origination of AE emission and earthquakes, some of the most widely used alternatives are inspired by geophysics. Four main approaches are outlined in the literature: the instantaneous amplitude (IA) threshold method [14], the short-term average to long-term average (STA/LTA) ratio [15], the Akaike information criterion (AIC) [16] and time-frequency distributions based on the continuous wavelet transform (CWT) [17].

Nevertheless, although these methods perform well for determining the onset time of transient AE signals, their performance for determining the signal endpoint and their efficiency in the case of a burst of AE events, remain unconcerned. Due to the lack of a common frame benchmarking, there are significant constraints on the widespread application of the four methods in non-destructive testing procedures, particularly fracture mechanism tests that could potentially be used to improve the methods.

Consequently, the contribution of this study is twofold: first, it identifies and analyses the main drawbacks and limitations of the classic threshold approach for AE detection; second, it offers a quantitative performance analysis of the main alternative methods currently available against a common benchmark of comparison.

Novelty of this work includes a comprehensive performance comparison of current AE hit detection methods, based on the scrutiny not only on their onset accuracies, but also in the endpoint and duration determinations, as well as in their statistical metrics. It should be noted that the performance of each method is verified against two test benches: first, a set of AE signals generated through a standardized Hsu-Nielsen test, and second, an AE signal obtained from a standardized tensile strength test. This is the first time that the IA, STA/LTA, AIC and time-frequency methods have been compared in the context of metallic material testing procedures for AE hit detection.

This paper is organized as follows: Section II presents a comprehensive analysis of the limitations of the classical AE threshold approach; Section III introduces the IA, STA/LTA, AIC and time-frequency methods; Section IV discusses the performance of the methods and experimental results, and Section V presents the conclusions.

II. ACOUSTIC EMISSION THRESHOLDING METHOD: LIMITATIONS AND DRAWBACKS

Although widely applied in many industrial applications, the thresholding approach used to detect and extract hits from an AE waveform presents some important shortcomings that must be identified in order to assess its suitability for high-performance applications. The main weaknesses of this method when dealing with AE signals, and their impact on the resulting AE hit detection, are presented and discussed below. The signals presented in this section were captured during unidirectional tensile tests (with a load rate of 1 mm/min). Each image corresponds to a different metallic component specimen, all of which have the same dimensions; height (h) = 240 mm, width (w) = 55 mm, and thickness (t) of 2 mm.

A. INABILITY TO DETECT BIPOLAR ONSET ACTIVITY

Only the positive part of the resulting electrical signal (or negative, according to the configuration) is considered for onset detection, as shown in Figure 1. The first motion direction (i.e., up or down) of an AE wave cannot be predicted deterministically, so depending on the chosen configuration for the threshold detector (i.e., rising or falling edge triggering), the onset times of a significant number of hits will be inaccurate. This is particularly relevant in damage location techniques where an accurate time of arrival or time of flight

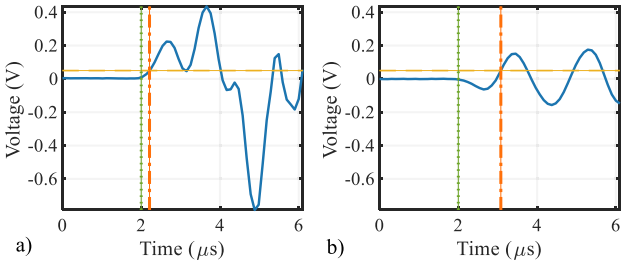

FIGURE 1. Actual onset (vertical dotted green line), and automatic onset determination (vertical dash-dot orange line) for two different AE events (solid blue lines) showing opposite *p*-wave arrival directions, using a positive threshold level (horizontal dashed yellow line) of 50mV. Signal obtained from a complex phase steel specimen.

(i.e., relative measurement time between elements of a sensor array) is crucial [18]. Alternatively, in the case of damage assessment methods (like those based on moment tensor inversion), information about the direction of the primary wave (i.e., *p*-wave) is essential [19], [20].

This problem can be lessened with the use of: *a*) secondary thresholds (i.e., positive and negative thresholds detecting in parallel); *b*) pre-trigger buffering, which considers a certain number of data samples before a detection at the cost of an inaccurate measure of the actual onset time, as well as adding the risk that the detection will overlap with a previous hit, and *c*) signal transformation towards a characteristic function (CF), where it is common to use hardware to work with a rectified voltage or by means of software to work with a simple absolute value function.

B. VARYING BACKGROUND NOISE INACCURACIES

Varying background noise may cause: (*i*) false detection, due to increasing noise, *(ii)* incomplete detection, due to increasing noise, and *(iii)* insufficient sensitivity to trigger a detection, due to decreasing noise. Acoustic emission waves are highly susceptible to noise and are therefore likely to exhibit dynamic behaviour during surveys, reducing detection quality due to the fixed threshold level.

Despite extensive research into noise treatment strategies for AE signals [21], [22], which can be applied before or after hit detection, the problem of varying noise during discrimination of AE activity remains inherent to the method when a fixed threshold value is used. Traditionally [23], and in recent studies [24], [25], this issue has been addressed by using a floating threshold (also known as an automatic, adaptive or smart threshold) whose value is continuously adapted to noise. To obtain a floating threshold, a simple moving-average filtered version of the raw signal acquired from the AE-sensor is typically used, and as in the case of the fixed threshold approach, a hit is detected when the raw signal rises above the new floating threshold level.

Ultimately, however, this technique does not solve the problem, since there is a trade-off between detection sensitivity and the capacity to avoid noise, according to the time segment value of the moving-average function. In the case of the use of extreme values, for a very short time frame, the new

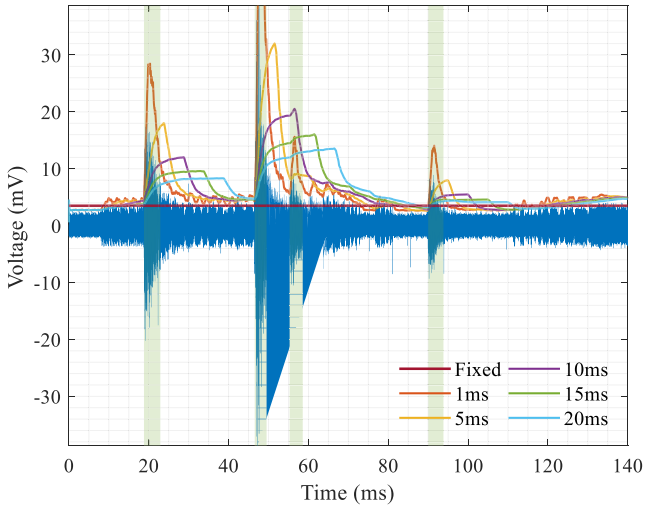

FIGURE 2. Five different floating threshold configurations on a highly noise-tainted data frame. Signal obtained from a TRIP bainitic ferrite and quenching-and-partitioning steel specimen.

threshold will behave as an envelope of the raw signal, avoiding all transient noises however inhibiting detection; if, however, it is too long, the floating threshold behaves as a fixed threshold. Consequently, this approach is best suited to applications in which background noise varies gradually; nevertheless, in applications prone to sudden mechanical noises (e.g., friction or slip) or with high AE activity it is difficult to find an optimum time response value [26], [27].

This, is depicted in Figure 2, for a 140 ms data frame containing four AE events, located at 18.8, 46.5, 55.2 and 90.0 ms, respectively (shaded green areas). First, it can be seen that a fixed threshold (horizontal red line), which is calibrated at 3.5 mV (just above the background noise level at the beginning of the signal frame) is not suitable in this instance, since after 8 ms a highly variable noise floor affects the signal, leading to a saturation detection error (except at around 80 and 110 ms, where the background noise returns to similar levels to the beginning of the data frame).

Additionally, five floating thresholds are implemented using a simple boxcar filter (zero-lag correction) for frame time configurations of 1 ms (orange curve), 5 ms (yellow curve), 10 ms (magenta curve), 15 ms (green curve) and 20 ms (cyan-blue curve) respectively. In this instance, although the floating thresholds clearly perform better than the fixed threshold, none of them completely solves the problem, since each one leads to its own detection errors.

This trade-off is evident in the case of the 1 and 5 ms configurations, where there is a choice between responding rapidly to non-transient background noise (achieved at 8.5 and 112 ms, respectively) and detecting more AE events than the slower configurations (third AE event located at 55 ms), but losing accuracy for determining the durations of all hits. By contrast, for longer time values, as in the case of the 10, 15 and 20 ms configurations, the determined durations are closer to the actual values (hits 1, 2 and 4). These configurations can also avoid some highly energetic transient

noises by being far from the noise floor (as at 30 and 75 ms), but at the cost of requiring too much time to respond to the variation in background noise (as can be observed for the time ranges 8.5–10 ms and 112–130 ms).

Finally, none of the configurations is capable of avoiding transient mechanical noises when the floating threshold value is close to the noise floor (as at 8.2, 76 and 111 ms).

C. RANDOMNESS OF EVENT INCIDENCE AND DURATION

The appearance and duration of AE events seem to behave stochastically during surveys. To address this, the fixed threshold technique is extended to include two time-driven parameters, hit definition time (HDT) and hit lockout time (HLT), which aim to prevent error detection, establishing a mechanism that determines the end of the event. However, and as in the above case of the floating threshold technique, these additional parameters imply a trade-off between detection sensitivity and robustness against errors.

Hit definition time, also known as duration discrimination time (DDT), uses a fixed timer to establish the end of a hit. Once a hit is detected, the system that implements the threshold technique will trigger the HDT timer with the condition that it restarts whenever the raw AE signal crosses the threshold level again before the time is complete.

However, the use of this timer also entails a latent risk in the quality of detection of AE activity, since it is impossible for a pre-set value to take into account the variety of durations (i.e., lifetime or lifespan of an AE wave) that the different hits will exhibit during a survey. In other words, a short pre-set duration will cause most of the identified hits to be truncated after detection and possibly split into two (or more) different events, whereas a long pre-set duration risks poses the risk of splicing the identification of two or more hits into a single event (sometimes misinterpreted as a cascaded hit).

Hit lockout time, also known as rearm time (RAT), aims to avoid the splicing of a detected hit with its own reflection, which is achieved by triggering the timer once the HDT reaches the end of its count. While HLT is active, the detector will not accept any further activity on the raw AE signal (whatever the nature is) until the HLT timer reaches the end of its count. The drawback of its implementation is that a short pre-set time will result in false-positive hit detection due to reflections or a split hit, while a long pre-set time will lead to the truncation or, in the worst case, the misdetection of a hit due to the risk that a hit will emerge during the HLT timing process [28].

Precise selection of the DHT and HLT timer values will obviously increase the detection accuracy of the threshold technique during a survey. However, even if instrumentation is carefully calibrated according to the characterization of the material under inspection (e.g., attenuation, speed of sound, etc.), the implementation of pre-set times will eventually induce errors as consequence of applying a fixed parameter to a stochastic phenomenon.

This trade-off is depicted in Figure 3, where two different AE event detection outputs are compared by slightly varying

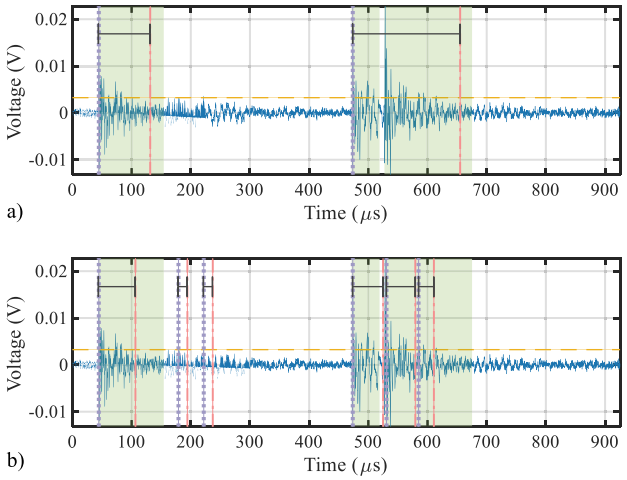

FIGURE 3. Two different outputs for the same AE frame signal, using two slightly different calibrations for the HDT and HLT parameters, and maintaining the same threshold level value (horizontal dashed yellow line) of 3.25mV. Automatic durations are indicated by the upper horizontal solid black guidelines. (a) Larger time values. (b) Smaller time values. Signal obtained from a ferrite-pearlite annealing steel specimen.

the HDT and HLT parameters for a 920 μs data frame. Shaded green areas indicate the actual durations of each of the hits found at 43.4, 471.5 and 527.3 μs, respectively. Vertical dotted lilac lines and vertical dash-dot pink lines, respectively, indicate the automatic onset and endpoint detections made by the conventional threshold technique.

The calibration shown in Fig. 3 (a) (HDT $=$ 40 μs, HLT $=$ 100 μs) is intended to achieve the best approximation for the durations of each hit, using higher timer values in order to reject detection errors caused by reflections of the hit. As can be observed, the selected values meet the objective, but at the cost of truncating the first hit (located at 43.4 μs and automatically detected after 1.2 μs), as well as splicing the second and third hits (471.5 and 527.3 μs, respectively) into a single event.

By contrast, the aim of the calibration shown in Fig. 3 (b) (HDT $=$ 15 μs, HLT $=$ 5 μs) is the timely detection of each hit. Thus, the highest timer values are used in order to identify the minimum required time difference in the values of the HDT and HLT parameters between calibrations. As can be observed, the onset of every hit is properly detected, but reflections of the hits are mistakenly detected as independent AE events. Moreover, the reflections of hits one and three are miss-detected as AE events.

D. HIGH DYNAMIC SIGNAL RANGE

The amplitudes of the AE waves will exhibit highly diverse scales, ranging from the order of picometres, giving rise to a transduced electrical signal that covers a range from millivolts to volts.

To address this issue it is a common practice to use a CF based on the logarithmic absolute value of the raw AE signal. This approach seeks to improve the calibration of the instrumentation by enhancing the visual deployment of the

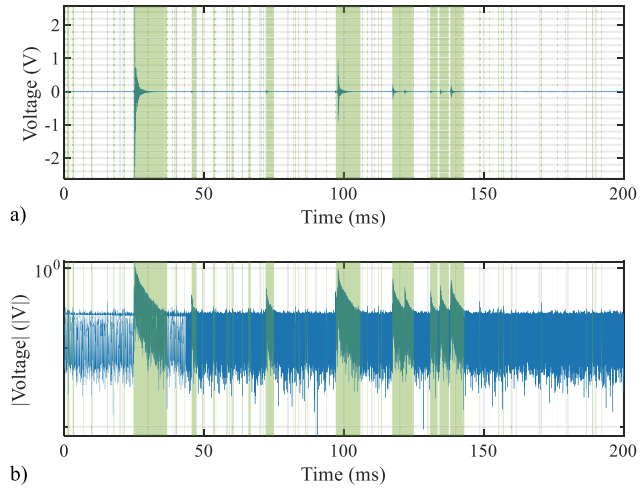

FIGURE 4. Differences in amplitude ranges of AE waves, for sixty-six AE events (durations indicated by shaded green areas). (a) Linear scale. (b) Same frame presented in a logarithmic scale. Signal obtained from a press hardening steel specimen.

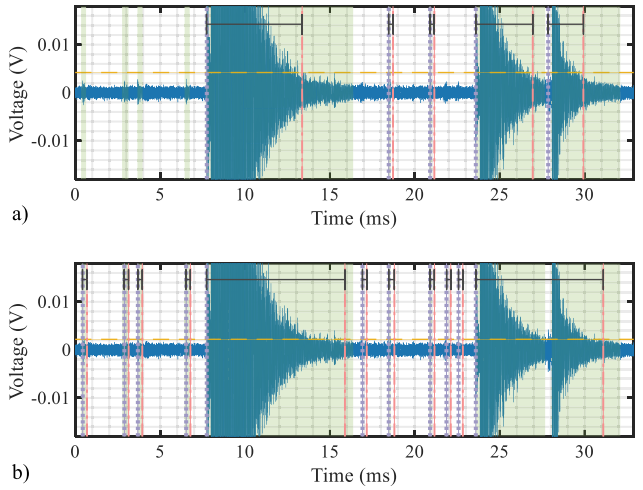

FIGURE 5. Output determinations of two slightly different calibrations for the threshold level value over the same AE frame signal. (a) 4.2mV, (b) 2.195mV. Voltage axis is zoomed in for a better depiction of the trade-off between calibrations.

signal to process, so that the level of the fixed threshold can be adjusted. By using this approach, the threshold level is typically given in decibels.

Figure 4 illustrates this approach, showing the same 200 ms data frame for a linear scale (a) and a logarithmic scale (b).

As can be observed, there is a significant difference between peak amplitudes for the different AE events, ranging from a minimum of 2.8 mV at 176.3 ms to a maximum of 2.6V at 25.3 ms. Figure 4 (a) shows that in a linear representation of the raw signal, only the most energetic events are discernible. In Figure 4 (b), having depicted the data frame on a logarithmic scale, it is less difficult to distinguish the different AE events.

Nevertheless, the use of this alternative approach still poses a risk to detection quality, as a fixed threshold is applied despite the large variance in the amplitudes of the AE events. This aspect leads to an additional trade-off when selecting the threshold value, forcing a choice between detection sensitivity and robustness to detection errors.

While it is true that increasing the threshold value reduces detection errors due to transient background noises, it also reduces detection sensitivity due to the loss of detection of the less energetic events and leads to inaccurate onset determination due to the misdetection of *p*-waves.

Conversely, reducing the threshold value increases detection sensitivity (since more AE events can be identified) as well as improving the accuracy of onset detection. Nevertheless, these improvements also raise susceptibility to false-positive detection errors (due to transient background noises, particularly those of a mechanical nature), as well as increasing the likelihood of splicing two or more hits into a single event.

This trade-off is illustrated in Figure 5, which compares two different output determinations of AE events by using two different threshold levels for the same 33 ms data frame. Shaded green areas indicate the actual durations for each of the nine hits found at 0.38, 2.75, 3.66, 6.44, 7.68, 18.42, 20.82, 23.59 and 28.06 ms, respectively, ranging from 2.795 mV (at 2.75 ms) to 2.5 V (at 7.65 ms).

Vertical dotted lilac lines and vertical dash-dot pink lines, respectively, represent automatic onset and endpoint detections. Both calibrations are set with the same HDT and HLT values of 250 μs and 400 μs, respectively. Automatically determined durations are also indicated by the upper horizontal solid black guidelines.

In Fig. 5 (a), the threshold level value is set at 4.2 mV, the aim of the calibration being to accurately determine the duration of the AE events while avoiding any false-positive detection. To achieve this, the threshold level is lowered to its minimum value before any error detection is generated. Although the approach achieves duration determinations close to the actual values, the number of AE events effectively detected is reduced considerably, with only five of the nine hits detected.

In Fig. 5 (b), this trade-off is highlighted by lowering the threshold level to the largest value that is required for detecting the nine existing AE events. As can be observed, each hit is detected effectively, but several transient noise events are mistakenly detected as hits, resulting in three false-positive events at 16.91, 21.86 and 22.57 ms. Moreover, events number eight and nine are spliced and detected as if they were a single event.

III. ADVANCED ACOUSTIC EMISSION HIT DETECTION METHODS

In order to overcome the limitations described above for AE hit detection based on the classical thresholding approach, some alternative CFs are implemented with the aim of avoiding the application of the threshold level to the raw signal, as is the case of the envelope of the signal by means of the absolute value function, as well as by the instantaneous

energy of the signal [15], [29]. Nevertheless, due to similarities in the origination of AE and earthquake phenomena, some of the most widely used methods are inspired by geophysics discipline (where these tools are known as phase pickers).

For this study, four advanced methodologies representative of the current literature were considered: IA, STA/LTA, AIC and time-frequency distribution methods.

One current trend is to build the CF by means of the Hilbert transform [14], [15], [30]. The aim of this approach is to obtain by means of the analytic signal of the captured data (preserving only the positive side of its frequency spectrum) a decomposition of the AE signal into two different time-variant components: instantaneous amplitude (IA) and instantaneous phase (IP). Instantaneous amplitude is of particular interest as it enables the construction of a CF that geometrically depicts the envelope of the AE wave with greater accuracy (in comparison to the conventional absolute value function). Once the CF has been obtained, the classic threshold scheme is applied. However, although under this scheme, uncertainties associated with the inability to detect bipolar onset activity are overcome; those related to background noise, randomness of the phenomenon and high dynamic range remain unaddressed.

The STA/LTA ratio picking method was proposed by Allen [31] for determining the onset time of earthquake events, with the aim of reducing false-positive alarms in seismic monitoring. First, a CF is obtained from the raw AE signal (typically an absolute value or its instantaneous energy), then each of the STA and LTA contributions derived from the CF is calculated by means of a moving average filter, with two different response times for each one. The short-term against long-term contributions of the CF are compared through the STA/LTA ratio, and then a fixed threshold level is applied directly to the ratio to detect AE hits. This reduces the influence of rapid events such as mechanical background noises, while maintaining a reasonably good response of the ratio in relation to the original signal. The drawback of this technique is the delay induced by the LTA contribution, which affects the precision of onset detection measurement, in particular losing detail for primary wave detection.

The AIC is a tool for statistically modeling time series, developed for automatic control applications by Akaike [32], first proposed by Maeda for seismic data [33], later implemented by Kurz [34] in the field of AE, and broadly revised by several authors of the AE discipline [18], [35]–[38]. It works by modeling the time series data of the raw AE signal under an autoregressive scheme (of low order). By estimating two locally stationary parametric components of the framed original signal (noise and AE activity); to later compare the entropy of each point of the modeled data, with the aim to find a critical point (the minimum). Thus, this critical point will indicate the arrival time instant of the AE wave.

Based on non-parametric signal processing methods, the time-frequency distribution analysis is a more accurate tool for detecting the onset time of AE waves. Using the short-time Fourier transform, Unnthorson proposed a fully automatic hit detector method [26], [39]. However, most current research focuses on the use of the wavelet transform (WT) [17], [40]–[43], which improves the resolution of the energy localization of the AE event in the time-frequency plane, increasing the accuracy of onset determination.

The AIC and CWT techniques clearly provide a more accurate onset determination of AE events than the classical threshold method, however, in a fully automatic AE hit detector application, typically they only serve to refine a coarsely detected hit (i.e., their use implies prior detection of the AE wave of interest). Clearly, this adds a degree of uncertainty to the outcome of these methods, since they will necessarily require an early thresholding detection framework.

Finally, it should be considered that although these advanced methods improve the detection accuracy for AE waves, the high data rates required to process the phenomenon make them computationally expensive, so they are usually implemented in an offline framework (first capturing the data of a survey, later extracting the AE events). Nevertheless, efforts have also been made to implement hardware architectures that can work in an online approach [44]–[46].

IV. PERFORMANCE OF ADVANCED ACOUSTIC EMISSION HIT DETECTION METHODS

As stated above, the most significant methods should be compared within a common analytical framework in order to establish a quantitative assessment of their performance. Consequently, based on the current literature, this study considers four AE detection methods: *a*) a classical threshold technique enhanced by the instantaneous amplitude component [14]; *b*) a typical STA/LTA [47]; *c*) a two-step AIC picker [16], and *d*) a CWT-Otsu detector over binary image mapping [17], which like *c*), uses the same function derived from Allen's formula as CF for the threshold-based preliminary detection.

Performance of methods is evaluated using two different datasets. First, to measure the precision of onset and endpoint detection, a collection of one-hundred different AE waves derived from a standardized Hsu-Nielsen test are processed by each method; then for each resulting outcome, the absolute detection errors are measured.

The second test bench measures the quality of event detection (i.e., accuracy, precision, false-positive rate, etc.) of each method using a data frame derived from a tensile test of a metallic component, which contains a wide variety (in terms of duration, amplitude and incidence) of AE waves.

For both experimental test benches, one sensor (Physical Acoustics WSα, 100-1000 kHz) was attached to the surface of each metallic component (using a silicon-based couplant). The resulting electrical signals were amplified (by a Mistras preamplifier 2/4/6) with a gain of 20 dB (BW 10–2500 kHz). The amplified electrical signals were recorded under a free-running sampling scheme (using a CSE4444 digitizer from GaGe), with a sampling frequency of 5 MHz for the Hsu-Nielsen data and 10 MHz for the tensile test data (both samplings with 16-bit depth resolution). Before processing

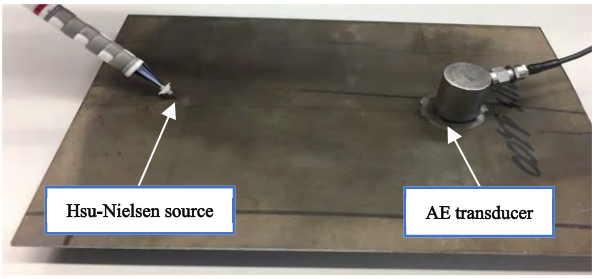

FIGURE 6. Standardised Hsu-Nielsen setup over a 1500 press hardening steel plate (guide-ring tube from Vallen Systeme).

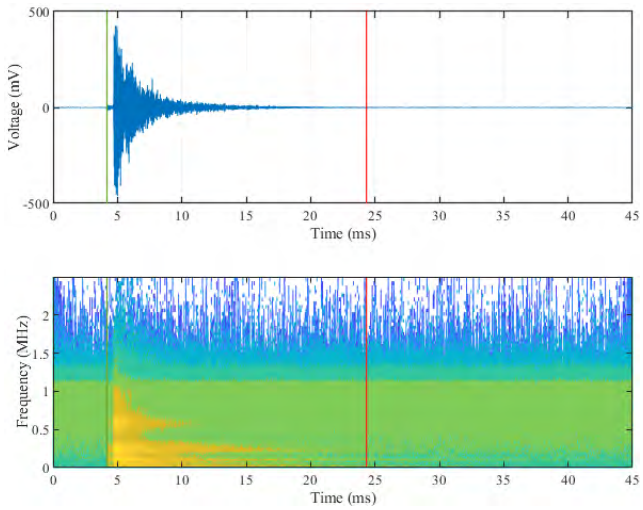

FIGURE 7. (a) Typical AE waveform analyzed in the synthetic data test bench. (b) Synchrosqueezed wavelet transform used to assist in the manual determination of the onset and endpoint pick locations of the AE wave (green and red vertical lines, respectively).

TABLE 1. Calibration parameter values for the Hsu-Nielsen test bench.

Parameter	Method			
	IA	*STA LTA*	*AIC*	*CWT Otsu*
Fixed threshold level	3e-3	5e-4	2e-1	2e-1
Hit definition time [µs]	1e3	NA	100	100
Hit lockout time [µs]	10e3	NA	10e3	10e3
De-trigger threshold	NA	9e-3	NA	NA
STA window time [µs]	NA	75	NA	NA
LTA window time [µs]	NA	1e6	NA	NA
Pre-event time [µs]	NA	15	NA	NA
Post-event time [µs]	NA	10e3	NA	NA
Weighting-R constant	NA	NA	4	4
End delay time window 1 [µs]	NA	NA	25	25
End delay time window 2 [µs]	NA	NA	10	NA
Start delay time window 1 [µs]	NA	NA	NA	1.5e3
Start delay time window 2 [µs]	NA	NA	100	NA
CWT scales	NA	NA	NA	101
Greyscale image bit-depth	NA	NA	NA	16
Median filter pixel neighbours	NA	NA	NA	50

TABLE 2. Absolute error and standard deviation for onset, endpoint and duration detections in the Hsu-Nielsen test bench.

Method	Onset time error (µs)	Endpoint time error (µs)	Duration time error (µs)
IA	-21.83 ± 8.26	2454 ± 1120	2476 ± 1120
STA/LTA	-19.82 ± 7.92	3828 ± 1159	3848 ± 1161
AIC	-13.34 ± 7.00	16338 ± 1045	16352 ± 1045
CWT-Otsu	-1.19 ± 97.88	17795 ± 1047	17796 ± 1039

the test bench, raw signals are band-pass filtered by using a FIR equiripple implementation (10–2200 kHz).

For each method, the most suitable calibration parameters for the test bench are set following the recommendations in the literature [16], [48]–[52] and in line with current standards [9], [10], [53]–[57]. Prior to performing the corresponding test benches, the onset and endpoint times of each of the AE waves were manually picked supported by time-voltage plots and a high-resolution time-frequency distribution [58].

A. HSU-NIELSEN DATA TEST BENCH

For the pencil-lead break test bench, for each of the one-hundred iterations, a graphite lead of ø 0.5 mm and 2.5 mm tip-length with a contact angle to the surface of 30° is used. A distance of 12 cm between source and sensor is maintained (see Figure 6).

For repeatability purposes, each synthetic AE wave is edited so that its peak value is centered on 5 ms and its length extends an additional 40 ms; a typical waveform obtained from this procedure is shown in Figure 7.

The objective of this test bench is to quantify the accuracy of each method in the measurement of onset, endpoint and duration times, by means of the absolute error of each measure. To assure accuracy, a strategy is used to calibrate the parameter values for each method, lowering the fixed threshold value to just above the background noise level for each characteristic function (see Table 1).

Since each method involves different signal-processing strategies, different CFs are obtained (except in the case of AIC and CWT-Otsu, and only for early detection). Thus, specific calibrations (i.e., threshold levels and timing values) are required for the selected technique (as reflected in Table 1). Once each of the methods has been applied to each synthetic AE wave, the accuracy of the onset, endpoint and duration times are quantified using the absolute error from the outcomes of the methods with respect to the manually selected time locations (see Table 2).

Table 2 shows that despite dealing with a challenging signal, by having to detect the AE onset when the *p*-wave arrives (which clearly has less amplitude than secondary waves), all methods perform relatively well for this detection stage, where in general terms the error is less than 20 μs for all cases. However, by executing a refinement of this onset examination, the AIC and CWT-Otsu methods present the lowest errors and can be considered to perform better.

Nevertheless, while the CWT-Otsu technique gives the lowest absolute error, it also shows the greatest dispersion values. The high accuracy and low precision can be attributed to the fact that the grayscale image derived from the CWT analysis of the signal (with which Otsu's method operates), when it contains a strong presence of either s-waves or noise regarding *p*-waves, tends to reduce the quality of the bimodal distribution of the image histogram, leading to segmentation errors. In the case of AIC, the inherent separation between noise and signal components, by means of finding the minimum in the calculated entropy of the raw signal, gives greater precision for the onset detection but at the cost of less accurate detections (i.e., lower dispersion error values but higher error detection values).

For the endpoint detection stage, all methods show poorer performance than for onset determination, which also has a direct effect on the estimation of the duration time. AIC and CWT-Otsu give nearly the same error values because they use the Allen's formula derivative as CF. However, IA and STA/LTA are the best options, reducing the average error of the AIC and CWT-Otsu methods by 80%.

As can be observed, the endpoint determination has not yet been satisfactorily resolved, since the absolute error is approximately 2–18 ms. This problem derives from the fact that instead of using a measure based on a tangible indicator extracted from the signal, in all of the methods endpoint determination is based on the combination of a fixed threshold and a fixed timer. Despite this drawback, the results also illustrate the advantage of obtaining a better representation of the signal through a more accurate CF, since although IA and STA/LTA also give significant endpoint determination errors, they can be considered to perform better thanks to lower absolute error values. In the case of IA this is achieved by a more responsive waveform, while in the case of STA/LTA, it is due to the consideration of future values of the signal with respect to current values.

B. FIELD DATA TEST BENCH

The objective of the second test bench is to quantify the quality of event detection for each method using field data.

This is carried out by means of a tensile test of a metallic component (see Fig. 8). The AE signal produced by the tensile test is recorded. For the field data test bench derived from this assay, a frame of 500 ms in length, containing 380 AE events (corresponding to an early damage stage of the specimen), is used as the input for each detection method (see Figure 9).

For this test bench, each of the AE events (as well as their onset and endpoint locations) is picked using the waveform of the frame and supported by its time-frequency distribution.

In comparison with the artificial AE events produced by the standardized Hsu-Nielsen procedure, real AE waves typically exhibit smaller amplitudes and shorter durations (depending, of course, on the damage stage of the specimen). Therefore, for the calibration used for this test bench (see Table 3), the time-driven parameters and the threshold level have been shortened to increase the sensitivity of the methods (with regard to temporal and amplitude detection capabilities).

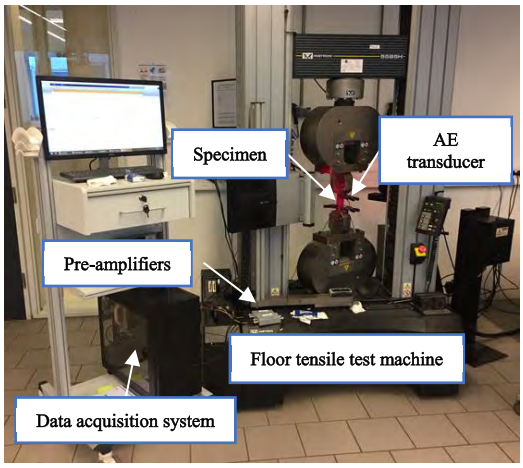

FIGURE 8. Standardised tensile test setup for a ferrite-pearlite annealing steel specimen (load rate of test 1mm/min).

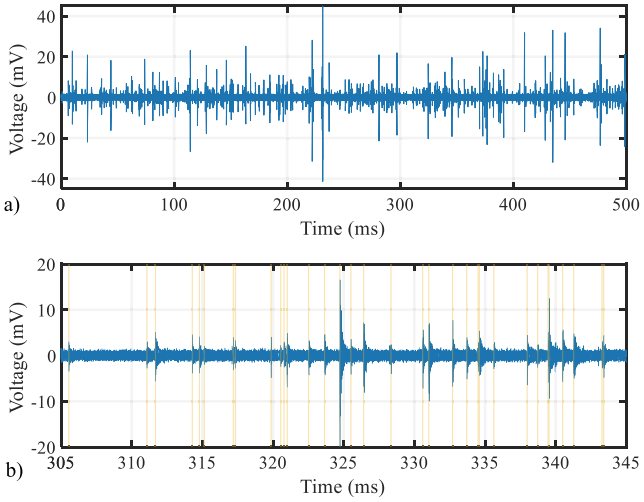

FIGURE 9. (a) Signal used for the field data test bench. (b) Zoom of 40ms, showing the variety in the incidence, duration and amplitudes of the AE waves present in the test bench (manual onsets indicated by vertical lines).

Once all of the methods have processed the field data frame, the quality of event detection is quantified in two steps. The first consists in quantifying the total number of detected events that each method concludes against the true locations of the 380 AE events. This step also inspects the sum of correctly detected events (true positive), the sum of undetected events (false negative) and the sum of the incorrectly detected events (false positive); see Table 4.

For this field data test bench, and only considering the total number of true positive events, the absolute errors for the onset, endpoint and duration are calculated (see Table 5).

Similar results are observed in the experimental scenario to those exhibited in the Hsu-Nielsen test bench. For the onset detection measure, all methods perform relatively well, showing in all cases error values of less than 10 μs, and with a difference among them of less than 7 μs.

TABLE 3. Calibration parameter values for the field data test bench.

Parameter	Method			
	IA	*STA LTA*	*AIC*	*CWT Otsu*
Fixed threshold level	2.25e-3	4e-3	6e-3	6e-3
Hit definition time [µs]	100	NA	100	100
Hit lockout time [µs]	15	NA	15	15
De-trigger threshold	NA	3e-3	NA	NA
STA window time [µs]	NA	25	NA	NA
LTA window time [µs]	NA	10e3	NA	NA
Pre-event time [µs]	NA	1	NA	NA
Post-event time [µs]	NA	0.5	NA	NA
Weighting-R constant	NA	NA	4	4
End delay window 1 [µs]	NA	NA	10	10
End delay window 2 [µs]	NA	NA	5	NA
Start delay window 1 [µs]	NA	NA	NA	75
Start delay window 2 [µs]	NA	NA	20	NA
CWT scales	NA	NA	NA	101
Greyscale image bit-depth	NA	NA	NA	16
Median filter pixel neighbours	NA	NA	NA	50

TABLE 4. Detected events with respect to 380 AE waves.

Number of events	Method			
	IA	*STA/LTA*	*AIC*	*CWT Otsu*
Detected	373	380	372	372
True-positive	322	324	299	299
False-negative	58	56	81	81
False-positive	51	56	73	73

TABLE 5. Absolute error and standard deviation for the onset, endpoint and duration detections with the field data test bench.

Method	Onset time error (µs)	Endpoint time error (µs)	Duration time error (µs)
IA	-9.69 ± 7.56	38.39 ± 101.27	48.09 ± 102.13
STA/LTA	-2.49 ± 8.63	12.07 ± 83.65	14.56 ± 84.85
AIC	-6.15 ± 10.44	19.57 ± 543.74	50.4 ± 692.6
CWT-Otsu	2.53 ± 29.45	-92.36 ± 97.4	89.82 ± 97.74

For the endpoint detection measure, the results are also consistent with the Hsu-Nielsen test bench, with all methods showing poorer performance than for onset detection. Nevertheless, STA/LTA seems to be the most balanced technique, particularly when dispersion error values are also taken into account, yielding values that are approximately 25–85% lower than the dispersion generated by IA and AIC, respectively. As can be seen, this endpoint error value also directly affects the absolute duration time error.

The second step in this field data test bench consists in quantifying the quality of event detection achieved by each method. Using the number of detected events shown in Table 4, the following statistical metrics are calculated:

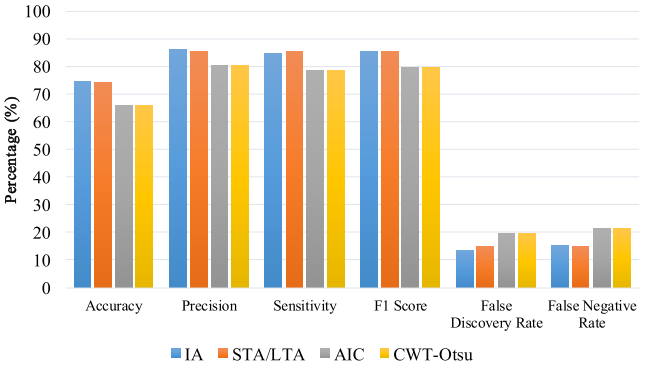

FIGURE 10. Statistical metrics corresponding to the quality of event detection in the data field test-bench.

(*a*) accuracy (the ratio of true positive events to all detected and undetected events), (*b*) precision (the ratio of true positive events to the number of true and false positive events), (*c*) sensitivity (the ratio of true positive events to the sum of true positive and false negative detections, (*d*) f1-score (the harmonic average of precision and sensitivity), (*e*) false discovery rate (the ratio of false positive detections to all detected events), (*f*) false negative rate (the ratio of false negative detections to the sum of false negative and true positive events).

With regard to the statistical metrics, Table 4 and Figure 10 show that although, on average, all of the methods quantitatively detect nearly 99% of the total detection target (i.e., 380 AE events), the quality with which these detections are performed still differs from the target.

Looking at the accuracy of the methods (i.e., the ratio of correctly detected events), although all of them perform reasonably well, with a lowest value of 66%, none achieves a value greater than 75%. STA/LTA and IA achieve accuracies nearly 10% greater than those of AIC and CWT-Otsu. This superior performance is consistent with the results obtained for the absolute endpoint error, since better determination of the event conclusion eventually raises the overall detection accuracy.

For the precision indicator (i.e., the ratio of correct positive detections) all methods perform better than for accuracy, achieving an average value of 83%. This improvement performance is due to the nature of the assay, in which there is a low proportion of false AE events (most of them derived from high-energy reflections and mechanical noises) relative to the number of true AE events in the analyzed data frame. Again, STA/STL and IA perform approximately 5% better than the AIC and CWT-Otsu methods, since they do not detect the false positive events for more cases in the test bench.

With regard to the sensitivity metric (i.e., the ratio of correctly detected positive events), all methods show similar behaviour to that observed for the precision metric, achieving nearly the same values. However, with the exception of STA/STL, performance decreases by about 2%, with a propensity for false negative detections, caused by low energy

AE events and, predominantly, by misdetection of spliced AE waves.

For the F1 score, all methods achieved satisfactory results, due to the fact that only minor deviations were obtained between the sensitivity and precision metrics.

For the false discovery rate metric (i.e., the ratio of false alarm detections), all methods show reasonably low values, completing the ratios observed for the precision metric, with the lowest value of 20% obtained by the AIC and CWT-Otsu techniques.

For the false negative rate (i.e., the proportion of actual events which do not produce detections), all methods show tolerable values consistent with the results for the sensitivity metrics, with the lowest value of 22% scored by the AIC and CWT-Otsu techniques.

V. CONCLUSIONS

Four critical characteristics influence the detection of AE events under the classical thresholding approach: bipolar onset activity, varying background noise, high dynamic signal range, and randomness in the incidence and duration of the events. The drawbacks and impacts of these characteristics have been discussed and analyzed.

Four advanced AE detection methods representing the current state of the art have been presented, and their performance quantified with AE data generated from standardized Hsu-Nielsen tests and for a standardized tensile test.

In general, all methods showed suitable capabilities for accurate onset detection, achieving absolute errors of less than 20 μs for the Hsu-Nielsen test and less than 10 μs for the tensile test.

By contrast, all methods exhibited low and nondeterministic performance for endpoint determination, yielding absolute errors of 2–18 ms for the Hsu-Nielsen test and 10–100 μs for the field data test bench. This lack of accuracy is due to the fact that all methods define the end of an event by means of the combination of a fixed threshold and a fixed timer instead of using an indicator extracted from the signal, which also critically increases the event duration error.

With regard to detection quality, none of the methods achieved an accuracy of more than 75%, with IA and STA/STL achieving scores approximately 10% higher than obtained with AIC and CWT-Otsu. For the precision and sensitivity metrics, due to the low proportion of false events in the test bench, all methods scored higher than for accuracy, achieving average scores of 83%. All methods were also found to be slightly more susceptible to false negative detection errors, most of them derived from spliced detections.

In general, statistical metrics are directly affected by the lack of accuracy of endpoint determination, and by four particular characteristics of the AE signal (i.e., duration, amplitude, appearance and floor noise).

In this study, AIC and CWT-Otsu are the best methods for accurate onset measurement. In particular, despite exhibiting significant error dispersions, CWT-Otsu improves onset measurement by approximately 90–95% with respect to all methods for the Hsu-Nielsen test and by 60 and 73% relative to AIC and IA, respectively, for the tensile test. Nevertheless, since these methods were conceived for AE event location applications, in which highly accurate event arrival times are critical, their scopes must be carefully considered to only refine this onset detection.

For this study, IA and STA/LTA can be considered the most suitable techniques for fully automatic AE event detection application, having achieved the highest scores for quality of detection analysis. This high performance is strongly related to the use of characteristic functions that are more suitable for detection purposes, which are more responsive in the case of IA and more accurate in the case of STA/LTA.

STA/LTA stands out in this study as the most balanced option between low-error accuracy for onset and endpoint determinations and the quality of detection metrics.

Finally, it should be noted that, due to the stochastic nature of the AE phenomenon, there is no overall method capable of guaranteeing reliable detection across all different applications, materials and instrumentation. Thus, careful consideration must be given to selecting the most suitable detection method for the performing environment in question.

For the further development of this topic, two branches can be defined. First, additional analysis of the performance of existing methods (such as the specificity of the threshold levels) and further experimental scenarios (such as in-service applications). Second, toward achieving meaningful and reliable AE assessing applications through the proper separation of each wave, the necessity of development of novel strategies that can determine more accurately not only the onset of an AE event but the conclusion as well.

REFERENCES

[1] J. Hirsch and T. Al-Samman, "Superior light metals by texture engineering: Optimized aluminum and magnesium alloys for automotive applications," *Acta Mater.*, vol. 61, no. 3, pp. 818–843, Feb. 2013.

[2] M. K. Kulekci, "Magnesium and its alloys applications in automotive industry," *Int. J. Adv. Manuf. Technol.*, vol. 39, nos. 9–10, pp. 851–865, Nov. 2008.

[3] *Standard Test Methods for Tension Testing of Metallic Materials*, Standard ASTM E8/E8M-13, 2016.

[4] *Metallic Materials—Tensile Testing—Part 1: Method of Test at Room Temperature*. Standard ISO 6892-1, ISO, Geneva, Switzerland, 2016, p. 79.

[5] L. Tian, L. Yu, and B. Pan, "Accuracy enhancement of a video extensometer by real-time error compensation," *Opt. Lasers Eng.*, vol. 110, pp. 272–278, Nov. 2018.

[6] E. Martinez-Gonzalez, I. Picas, D. Casellas, and J. Romeu, "Detection of crack nucleation and growth in tool steels using fracture tests and acoustic emission," *Meccanica*, vol. 50, no. 5, pp. 1155–1166, May 2015.

[7] E. D. Merson, P. N. Myagkikh, G. V. Klevtsov, D. L. Merson, and A. Vinogradov, "Effect of fracture mode on acoustic emission behavior in the hydrogen embrittled low-alloy steel," *Eng. Fract. Mech.*, vol. 210, pp. 342–357, Apr. 2018.

[8] C. J. Hellier, "Acoustic emission testing," in *Handbook of Nondestructive Evaluation*, 2nd ed. New York, NY, USA: McGraw-Hill, 2013.

[9] *Standard Practice for Characterizing Acoustic Emission Instrumentation*, Standard ASTM E750-15, ASTM, West Conshohocken, PA, USA, 2015.

[10] *Non-Destructive Testing—Acoustic Emission Inspection*. Standard ISO 12716, 2017.

[11] J. Hensman, R. Mills, S. G. Pierce, K. Worden, and M. Eaton, "Locating acoustic emission sources in complex structures using Gaussian processes," *Mech. Syst. Signal Process.*, vol. 24, no. 1, pp. 211–223, Jan. 2010.

[12] Z. Zhou, Y. Rui, J. Zhou, L. Dong, and X. Cai, "Locating an acoustic emission source in multilayered media based on the refraction path method," *IEEE Access*, vol. 6, pp. 25090–25099, 2018.

[13] S. A. Shevchik, B. Meylan, A. Mosaddeghi, and K. Wasmer, "Acoustic emission for *in situ* monitoring of solid materials pre-weakening by electric discharge: A machine learning approach," *IEEE Access*, vol. 6, pp. 40313–40324, 2018.

[14] E. D. Niri, A. Farhidzadeh, and S. Salamone, "Nonlinear Kalman Filtering for acoustic emission source localization in anisotropic panels," *Ultrasonics*, vol. 54, no. 2, pp. 486–501, Feb. 2014.

[15] M. Ohtsu, M. Enoki, Y. Mizutani, and M. Shigeishi, "Principles of the acoustic emission (AE) method and signal processing," in *Practical Acoustic Emission Testing*. Tokyo, Japan: Springer, 2016, p. 130.

[16] P. Sedlak, Y. Hirose, and M. Enoki, "Acoustic emission localization in thin multi-layer plates using first-arrival determination," *Mech. Syst. Signal Process.*, vol. 36, no. 2, pp. 636–649, Apr. 2013.

[17] F. Bai, D. Gagar, P. Foote, and Y. Zhao, "Comparison of alternatives to amplitude thresholding for onset detection of acoustic emission signals," *Mech. Syst. Signal Process.*, vol. 84, pp. 717–730, Feb. 2017.

[18] S. K. Al-Jumaili, M. R. Pearson, K. M. Holford, M. Eaton, and R. Pullin, "Acoustic emission source location in complex structures using full automatic delta T mapping technique," *Mech. Syst. Signal Process.*, vols. 72–73, pp. 513–524, May 2016.

[19] T. S. Eyre and M. van der Baan, "Overview of moment-tensor inversion of microseismic events," *Lead. Edge*, vol. 34, no. 8, pp. 882–888, Aug. 2015.

[20] T. Schumacher, D. Straub, and C. Higgins, "Toward a probabilistic acoustic emission source location algorithm: A Bayesian approach," *J. Sound Vib.*, vol. 331, no. 19, pp. 4233–4245, Sep. 2012.

[21] X. Chiementin, D. Mba, B. Charnley, S. Lignon, and J. P. Dron, "Effect of the denoising on acoustic emission signals," *J. Vib. Acoust.*, vol. 132, no. 3, Apr. 2010, Art. no. 031009.

[22] L. Calabrese, G. Campanella, and E. Proverbio, "Noise removal by cluster analysis after long time AE corrosion monitoring of steel reinforcement in concrete," *Construct. Building Mater.*, vol. 34, pp. 362–371, Sep. 2012.

[23] I. F. M. Carroll, "Automatic threshold control means and the use thereof," U.S. Patent 4 036 057, Jul. 19, 1977.

[24] D. D. Doan, E. Ramasso, V. Placet, S. Zhang, L. Boubakar, and N. Zerhouni, "An unsupervised pattern recognition approach for AE data originating from fatigue tests on polymer—Composite materials," *Mech. Syst. Signal Process.*, vols. 64–65, pp. 465–478, Dec. 2015.

[25] D. Xiang, "Acoustic emission detection of early stages of cracks in rotating gearbox components," in *Proc. AIP Conf.*, 2017, p. 1806.

[26] R. Unnthorsson, T. P. Runarsson, and M. T. Jonsson, "Acoustic emission based fatigue failure criterion for CFRP," *Int. J. Fatigue*, vol. 30, no. 1, pp. 11–20, Jan. 2008.

[27] V. Barat, D. Grishin, and M. Rostovtsev, "Detection of AE signals against background friction," *J. Acoustic Emission*, vol. 29, pp. 133–141, Jan. 2011.

[28] K. Ito and M. Enoki, "Acquisition and analysis of continuous acoustic emission waveform for classification of damage sources in ceramic fiber mat," *Mater. Trans.*, vol. 48, no. 6, pp. 1221–1226, 2007.

[29] C. U. Grosse and M. Ohtsu, *Acoustic Emission Testing: Basics for Research—Applications in Civil Engineering*. Berlin, Germany: Springer, 2008.

[30] K. Nadolny, P. Sutowski, and D. Herman, "Analysis of aluminum oxynitride AlON (Abral) abrasive grains during the brittle fracture process using stress-wave emission techniques," *Int. J. Adv. Manuf. Technol.*, vol. 81, nos. 9–12, pp. 1961–1976, Dec. 2015.

[31] R. V. Allen, "Automatic earthquake recognition and timing from single traces," *Bull. Seismol. Soc. Amer.*, vol. 68, no. 5, pp. 1521–1532, 1978.

[32] H. Akaike, "A new look at the statistical model identification," *IEEE Trans. Autom. Control*, vol. 19, no. 6, pp. 716–723, Dec. 1974.

[33] N. Maeda, "A method for reading and checking phase time in auto-processing system of seismic wave data," *Zisin*, vol. 38, no. 3, pp. 365–379, 1985.

[34] J. H. Kurz, C. U. Grosse, and H.-W. Reinhardt, "Strategies for reliable automatic onset time picking of acoustic emissions and of ultrasound signals in concrete," *Ultrasonics*, vol. 43, no. 7, pp. 538–546, Jun. 2005.

[35] C. C. Graham, S. Stanchits, I. G. Main, and G. Dresen, "Comparison of polarity and moment tensor inversion methods for source analysis of acoustic emission data," *Int. J. Rock Mech. Mining Sci.*, vol. 47, no. 1, pp. 161–169, Jan. 2010.

[36] P. Sedlak, Y. Hirose, S. A. Khan, M. Enoki, and J. Sikula, "New automatic localization technique of acoustic emission signals in thin metal plates," *Ultrasonics*, vol. 49, no. 2, pp. 254–262, Feb. 2009.

[37] A. Ebrahimkhanlou and S. Salamone, "Acoustic emission source localization in thin metallic plates: A single-sensor approach based on multimodal edge reflections," *Ultrasonics*, vol. 78, pp. 134–145, Jul. 2017.

[38] K. M. Holford, M. J. Eaton, J. J. Hensman, R. Pullin, S. L. Evans, N. Dervilis, and K. Worden, "A new methodology for automating acoustic emission detection of metallic fatigue fractures in highly demanding aerospace environments: An overview," *Prog. Aerosp. Sci.*, vol. 90, pp. 1–11, Apr. 2017.

[39] R. Unnthorsson, "Hit detection and determination in AE bursts," in *Acoustic Emission— Research and Applications*, Rijeka, Croatia: InTech, 2013, pp. 1–20.

[40] D. Bianchi, E. Mayrhofer, M. Gröschl, G. Betz, and A. Vernes, "Wavelet packet transform for detection of single events in acoustic emission signals," *Mech. Syst. Signal Process.*, vols. 64–65, pp. 441–451, Dec. 2015.

[41] A. Gupta and J. C. Duke, Jr., "Identifying the arrival of extensional and flexural wave modes using wavelet decomposition of ultrasonic signals," *Ultrasonics*, vol. 82, pp. 261–271, Jan. 2018.

[42] E. Pomponi, A. Vinogradov, and A. Danyuk, "Wavelet based approach to signal activity detection and phase picking: Application to acoustic emission," *Signal Process.*, vol. 115, pp. 110–119, Oct. 2015.

[43] A. Danyuk, I. Rastegaev, E. Pomponi, M. Linderov, and D. Merson, "Improving of acoustic emission signal detection for fatigue fracture monitoring," *Procedia Eng.*, vol. 176, pp. 284–290, Jan. 2017.

[44] M. Kang, J. Kim, and J. M. Kim, "An FPGA-based multicore system for real-time bearing fault diagnosis using ultrasampling rate AE signals," *IEEE Trans. Ind. Electron.*, vol. 62, no. 4, pp. 2319–2329, Apr. 2015.

[45] S. Wirtz, A. Cunha, M. Labusch, G. Marzun, S. Barcikowski, and D. Söffker, "Development of a low-cost FPGA-based measurement system for real-time processing of acoustic emission data: Proof of concept using control of pulsed laser ablation in liquids," *Sensors*, vol. 18, no. 6, p. 1775, Jun. 2018.

[46] Y. Hu, L. Wang, X. Huang, X. Qian, L. Gao, and Y. Yan, "On-line sizing of pneumatically conveyed particles through acoustic emission detection and signal analysis," *IEEE Trans. Instrum. Meas.*, vol. 64, no. 5, pp. 1100–1109, May 2015.

[47] P. Bormann, Ed., *New Manual of Seismological Observatory Practice (NMSOP-2)*. Potsdam, Germany: Deutsches GeoForschungszentrum GFZ; IASPEI, 2012. doi: 10.2312/GFZ.NMSOP-2.

[48] K. Ono, "Calibration methods of acoustic emission sensors," *Materials*, vol. 9, no. 7, p. 508, Jul. 2016.

[49] N. M. Nor, A. Ibrahim, N. M. Bunnori, H. M. Saman, S. N. M. Saliah, and S. Shahidan, "Diagnostic of fatigue damage severity on reinforced concrete beam using acoustic emission technique," *Eng. Failure Anal.*, vol. 41, pp. 1–9, Jun. 2014.

[50] G. C. McLaskey and D. A. Lockner, "Calibrated acoustic emission system records M–3.5 to M–8 events generated on a saw-cut granite sample," *Rock Mech. Rock Eng.*, vol. 49, no. 11, pp. 4527–4536, Nov. 2016.

[51] D. Fettré, J. Favergeon, and S. Bouvier, "Detection of breakaway for a high-temperature oxidation of pure zirconium using acoustic emission correlated to thermogravimetry," *Oxidation Met.*, vol. 87, nos. 3–4, pp. 367–379, Apr. 2017.

[52] E. D. Niri, A. Farhidzadeh, and S. Salamone, "Determination of the probability zone for acoustic emission source location in cylindrical shell structures," *Mech. Syst. Signal Process.*, vols. 60–61, pp. 971–985, Aug. 2015.

[53] *Standard Guide for Determining the Reproducibility of Acoustic Emission Sensor Response*, Standard ASTM E976-15, ASTM, 2015.

[54] *Standard Guide for Mounting Piezoelectric Acoustic Emission Sensors*, Standard ASTM E650/E650M-17, ASTM, 2017.

[55] *Standard Guide for Acoustic Emission System Performance Verification*, Standard ASTM E2374-16, ASTM, 2016.

[56] *Standard Guide for Acoustic Emission Examination of Small Parts*, Standard ASTM E1932-12, ASTM, 2017.

[57] *Standard Test Method for Primary Calibration of Acoustic Emission Sensors*, Standard ASTM E1106-12, ASTM, 2017.

[58] I. Daubechies, J. Lu, and H. T. Wu, "Synchrosqueezed wavelet transforms: An empirical mode decomposition-like tool," *Appl. Comput. Harmon. Anal.*, vol. 30, no. 2, pp. 243–261, Mar. 2011.

FERNANDO PIÑAL MOCTEZUMA (S'13) was born in Puebla, México. He received the B.Sc. and M.Eng. degrees in electronics from the Autonomous University of Puebla, Mexico, in 2008 and 2013, respectively. He is currently pursuing the Ph.D. degree in electronics engineering with the Universitat Politècnica de Catalunya (UPC), Spain. His current research interests include instrumentation and measurement systems, and the methods of damage assessment and signal processing for the acoustic emission phenomenon.

MIGUEL DELGADO PRIETO (S'08–M'12) was born in Barcelona, Spain, in 1983. He received the Ph.D. degree in electronics engineering from the Universitat Politècnica de Catalunya (UPC), Barcelona, Spain, in 2012. Since 2008, he has been a Researcher with the MCIA Research Center and an Adjunct Lecturer with the Electronic Engineering Department with UPC. He is currently involved in research, technology transfer and project management activities around condition-based monitoring, and the Internet of Things for the industry, energy, and transport sectors. His research interests include instrumentation, signal processing, and machine learning methods.

LUIS ROMERAL MARTÍNEZ (M'98) received the M.S. degree in electrical engineering and the Ph.D. degree from the Universitat Politècnica de Catalunya (UPC), Barcelona, Spain, in 1985 and 1995, respectively. In 1988, he joined the Electronic Engineering Department, UPC, where he is currently an Associate Professor and the Director of the Motion and Industrial Control Group, the major research activities of which concern induction and permanent-magnet motor drives-based applications, enhanced efficiency drives, fault detection, and the diagnosis of electrical motor drives and instrumentation and measurements based on different physical magnitudes.